Influence of cell temperature on water removal mechanism during shutdown purge in proton exchange membrane fuel cells

Experimental and simulation analysis

Zhang, Zhenya; Wei, Houyu; Lou, Taishan; Zhang, Jun; Xiao, Yanqiu; Jin, Tingxiang; Tian, Jiean; Li, Xuewei; Liu, Zhengxuan

DOI
10.1016/j.icheatmasstransfer.2024.108071

Publication date
2024

Document Version
Final published version

Published in
International Communications in Heat and Mass Transfer

International Communications in Heat and Mass Transfer 159 (2024) 108071

Contents lists available at ScienceDirect

International Communications in Heat and Mass Transfer

journal homepage: www.elsevier.com/locate/ichmt

Influence of cell temperature on water removal mechanism during shutdown purge in proton exchange membrane fuel cells: Experimental and simulation analysis

Zhenya Zhang [a], Houyu Wei [a], Taishan Lou [b], Jun Zhang [a], Yanqiu Xiao [a], Tingxiang Jin [a], Jiean Tian [c], Xuewei Li [c], Zhengxuan Liu [d,*]

[a] School of Energy and Power Engineering, Zhengzhou University of Light Industry, Henan Province, Zhengzhou 450001, China
[b] School of Electrical and Information Engineering, Zhengzhou University of Light Industry, Henan Province, Zhengzhou 450001, China
[c] G-Power Technology (Shanghai) Co., Ltd., Shanghai 201800, China
[d] Faculty of Architecture and the Built Environment, Delft University of Technology, Julianalaan 134, 2628 BL Delft, Netherlands

ARTICLE INFO

Keywords:
Proton exchange membrane fuel cell
Shutdown purge mechanism
Cell temperature
Water phase change
Water content

ABSTRACT

The internal temperature of proton exchange membrane fuel cells significantly influences their shutdown purge process a key factor for ensuring operational stability and longevity. This study explores how cell temperature impacts water removal mechanisms during shutdown purge, emphasizing its importance for the operational stability of fuel cell. High-temperature purge experiments were conducted using an integrated stack experimental platform, revealing that prolonged high-temperature purging increased the high frequency resistance of a single cell to 639.44 $m\Omega \bullet cm^2$ and caused severe perforation of the membrane electrode assembly. To delve deeper into the mechanisms of cell temperature influence and the cause of perforation, an isothermal, transient, two-phase flow fuel cell model was developed. The cell temperature during purge was incrementally raised from 303.15 K to 358.15 K in 5 K steps. Detailed analyses of membrane desorption and water phase changes during purge processes were performed. At cell temperatures ranging from 338.15 K to 358.15 K, a 120-s purge reduced the membrane water content to below 4.8, with only a 5 % variation in residual membrane water. When the cell temperature exceeded 323.15 K, water activity increased with temperature, intensifying evaporation and leading to desorption of vapor from the membrane. Consequently, higher temperatures facilitated the removal of liquid water, with no liquid water remaining within cell above 323.15 K. Elevated cell temperatures accelerated the purge, resulting in lower liquid water content and increased vapor, but with minimal difference in membrane water content. The intense evaporation process and rapid purge at high temperatures were identified as direct causes of membrane electrode assembly perforation. This study highlights the critical role of cell temperature in the shutdown purge process, providing innovative insights into optimizing proton exchange membrane fuel cell operations for enhanced performance and durability.

1. Introduction

Proton exchange membrane fuel cells (PEMFCs) is a promising clean energy technology that efficiently converts chemical energy into electrical energy through electrochemical reactions [1]. Efficient water management is essential for improving the efficiency and reliability of PEMFCs due to the significant presence of water during energy conversion [2]. Water management strategies typically focus on maintaining a dynamic balance between water production and removal [3]. This balance is greatly influenced by the operating conditions, especially during the start-stop cycles of the cell [4]. When the fuel cell is operated at sub-freezing temperatures, the residual water inside the cell after shutdown freezes into ice, blocking mass transfer channels and covering reaction sites, ultimately leading to failure of cold start [5–7]. Thus, purging excess water during the shutdown process is a crucial method for optimizing water management [8,9].

Current research on shutdown purge primarily focuses on optimizing purge conditions and strategies, including the type of purge gas, temperature, relative humidity (RH), flow rate, pressure, and purge current density [10]. The gases used for shutdown purges include nitrogen, air, and hydrogen. Introducing a small amount of hydrogen into the cathode

* Corresponding author.
E-mail address: Z.liu-12@tudelft.nl (Z. Liu).

https://doi.org/10.1016/j.icheatmasstransfer.2024.108071

Available online 17 September 2024

Nomenclature

A	Fuel cell effective area, m^2
C	Molar concentration, mol/m^3
D	Gas diffusion coefficient, m^2/s
F	Faraday constant, C/mol
hm	Convection mass-transport coefficient, m/s
H	Thickness, m
i	Current density, mA/cm^2
J	Mass-transfer flux, $mol/(m^2 \bullet s)$
k	Phase change coefficient
K	Permeability, m^2
L	Length, m
q_l	Mass flow rate, kg/s
M	Molar mass, kg/mol
P	Pressure, Pa
r	Resistance, Ω
R	Gas constant, $J/(kg \bullet K)$
RH	Relative humidity, %
s	Liquid water saturation
T	Temperature, K
u	Flow velocity, m/s
U	Voltage, V
v	Kinematic viscosity, m^2/s
V	Volume, m^3
w	Weighting coefficient

Greek letters

α	Transfer coefficient
γ	Membrane water conversion rate, s^{-1}
ε	Porosity
η	Overpotential, V
θ	Contact angle, °
λ	Membrane water content
μ	Dynamic viscosity, $kg/(m \bullet s)$
ν	Voltage loss, V
ρ	Density, kg/m^3
σ	Surface tension, n/m

Subscripts

a	Anode
acl	Anode catalyst layer
act	Activation polarization
ccl	Cathode catalyst layer
cgc	Cathode gas channel
cl	Catalyst layer
conc	Concentration polarization
e	Electron conduction
eq	Equilibrium
evap	Evaporation
fc	Fuel cell
g	Gas
gc	Gas channel
gdl	Gas diffusion layer
in	Inlet
l	Liquid water
mem	Membrane
ohmic	Ohmic polarization
out	Outlet
p	Proton conduction
ref	Reference
sat	Saturation
v	Water vapor

can enhance purge performance, particularly in removing residual water from the cathode catalyst vicinity [11]. However, directly introducing hydrogen into the cathode may cause undesirable effects. Although purging with nitrogen can be equally effective [12], incorporating an additional nitrogen purge mechanism increases system complexity. Consequently, studies on shutdown purge for PEMFCs typically utilize air to purge the cathode, especially in systems designed for onboard fuel cells.

The purge temperature affects the purge process primarily by influencing the saturated vapor pressure [13]. The study of purge temperature is divided into gas temperature and cell temperature. Lower temperature purge gases carry more water when flowing through a hot cell [14]. Higher cell temperatures increase the saturated vapor pressure, facilitating the evaporation and discharge of liquid water [15]. Regarding the RH of the purge gas, lower RH is more favorable for removing liquid water and water vapor from the cell. Conversely, higher RH can cause water redistribution within the cell at the end of the purge and may even lead to the formation of liquid water [16]. Increasing the purge gas flow rate can significantly reduce purge time and enhance purge efficiency [17], but it increases energy consumption [18]. Notably, the remaining water volume in the membrane post-purge is unaffected by the flow rate [19]. For purge gas pressure, both excessively high and low pressures are unfavorable for removing liquid water inside the cell [17]. However, using the pressure mutation method can leverage the pressure difference to expel residual water [20]. The current density during purge must be appropriate. Excessively high purge current density generates too much water, impairing the purge effect, while too low a current density can cause high potentials, resulting in irreversible cell damage [18]. These studies on purge strategies provide strong theoretical support for improving the shutdown purge performance of PEMFCs.

However, in-depth analyses of the water removal mechanism during the purge process remain limited due to the complexity of water state and transport in different media [21]. It is generally accepted that water within a porous medium is primarily influenced by the coupled effects of surface evaporation and differential pressure [19,22], with the dominance of these effects depending on the material properties [23]. The entire water removal process during shutdown purge can be divided into three phases: the slow-rise phase (SRP), the fast-rise phase (FRP), and the membrane equilibrium phase (MEP). The transitions between these phases are primarily determined by the complete removal of liquid water from the cell and the significant change in water content within the membrane [24]. Water phase changes play an important role throughout the purge process, and temperature is crucial in affecting these phase changes.

There are still significant gaps in understanding the effects of cell temperature during shutdown purge, primarily in the following aspects:

(1) Most experimental studies of the purge process have used mild operating parameters, lacking direct evidence and analysis of damage at the stack level under harsh purge conditions.
(2) Studies on cell temperature during purge have not fully analyzed the deeper effects of temperature on the overall water removal mechanism, particularly from the perspective of water phase changes and to consider the tolerance of the purge process to temperature variations.
(3) In automotive PEMFC systems, shutdown purge must be completed quickly. However, too rapid a purge can damage the cell. Therefore, formulating a shutdown purge strategy requires

balancing the need for quick shutdown with the safety of the PEMFC system to minimize cell damage.

In this study, a comprehensive experimental platform with 450 cells is used to conduct long-duration, high-temperature purges to examine the effects of harsh purge conditions on the purge process and potential damage to the stack. Additionally, to further investigate the causes of high-temperature damage to the cells and to deeply analyze the influence of cell temperature on the water removal mechanism during purge, an isothermal, transient, two-phase flow PEMFC model based on the MATLAB/SIMULINK platform is employed. The purge curve of the water in the cell at different temperatures and the residual water content after 120 s of purge were obtained. The effect of cell temperature on the purge process is analyzed by focusing on the impact of temperature on water phase transitions, including the desorption of membrane water and gas-liquid transitions. Finally, by combining the effects of various factors, this paper identifies the optimal cell temperature during the purge process, providing a theoretical basis for future research on the mechanisms of internal water phase transitions and temperature control strategies during the purge process.

2. Experimental testing and simulation model development

2.1. Experimental platform and testing

The experimental platform uses a PEMFC stack with a rated power of 135 kW, consisting of 450 single cells with an active area of 250 cm^2 connected in series. The experimental platform and its schematic principle are shown in Fig. 1.

As depicted in Fig. 1, the PEMFC experimental platform includes an air system, a hydrogen system, a cooling water system, and an electrical system. The air system comprises an air compressor, an intercooler, and a membrane humidifier. The hydrogen system consists of a hydrogen supply device, a heat exchanger, an ejector, a water distributor, and a tail pipe. The cooling water system includes pumps, heat exchangers, PTCs, tanks, and deionizers. The electrical system includes DC-DC converters and external electronic loads. Humidity, pressure, flow, and temperature sensors are placed at specific locations within the system.

To investigate the purge performance of the PEMFC, a shutdown purge operation on the stack after it had been in stable operation was conducted for a period of time. The operating parameters are shown in Fig. 2.

After the fuel cell enters the shutdown process, the throttle of the air path is quickly adjusted so that the air flow rate enters into a purge flow rate of 260 kg/h within 20 s. The air inlet pressure simultaneously drops rapidly to a purge pressure of 23 kPa, and the hydrogen pressure follows to 40 kPa, at which time the purge metering ratio of the air is about 16, and the air temperature slowly decreases during the purge process. Further, in order to better analyze the effect of the stack temperature on the purge performance, the thermostat was turned off to maintain a high stack temperature when the purge reached about 150 s, and the purge time was extended to 292 s. The air pressure was then reduced to about 16 kPa, and the hydrogen pressure followed to 40 kPa.

2.2. Model development and validation

2.2.1. Physical model

The model in this paper is a reduced dimensional isothermal model and the model domain is shown in Fig. 3. The five-layer membrane electrode (MEA) of this model contains: anodic gas diffusion layer (AGDL), anodic catalyst layer (ACL), proton exchange membrane (PEM), cathodic catalyst layer (CCL), and cathodic gas diffusion layer (CGDL). And, there are also flow channels on both sides: anodic flow channel (AGC), cathodic flow channel (CGC), and the positive direction of the model is defined as from AGC to CGC. Among them, the key parameters calculating the mass transfer process within the PEMFC were the water concentration within the AGC C_{agc}, at the AGC-AGDL interface C_0, at the AGDL-ACL interface C_1, at the CCL-CGDL interface C_5, at the CGDL-CGC interface C_6, water concentration within the CGC C_{cgc}, the membrane water content within the ACL electrolyte λ_2, within the PEM λ_3, within the CCL electrolyte λ_4, liquid water saturation within the porous medium on the cathode side s_5, transported water flux within the AGDL J_a, between the ACL and the PEM electrolyte $J_{mem.acl}$, between the CCL and the PEM electrolyte $J_{mem.ccl}$, within the CGDL J_c.

In order to simplify the model calculations, several special assumptions need to be formulated. The modelling assumptions in this paper are as follows:

(1) The temperature of each component within the PEMFC is uniform and equal;
(2) Neglect the effect of gravity on the system;
(3) Fluid flow is laminar and incompressible;
(4) The porous medium is a hydrophobic material;
(5) Liquid water is only likely to occur within the CCL and CGDL.

2.2.2. Mathematical modelling and experimental validation

The mathematical model used in this paper is a reduced-dimensional model developed in our previous work [25] based on the studies by Hu et al. [26] and Xu et al. [27]. Parameters of the PEMFC concerned in this study are listed in Table 1. Additionally, the model has been validated by a purge experiment in our prior work [25]. The steady-state model was validated using an I-V curve, and the purge model was validated using a high-frequency resistance (HFR) curve. The simulated data from the steady-state model show good agreement with the experimental data: all the simulated I-V curve data deviate by less than 5 % from the experimental data, with an average error of 1.39 %. Similarly, most of the simulated HFR curve data deviate by less than 5 %, and all deviations are under 10 %, with an average error of 4.17 %. This agreement confirms the feasibility of the simulations within the allowable error. A brief review of the important equations involved in the model is presented.

Assuming that the distribution of water content within the electrolyte is segmentally linear, the membrane water transports are expressed as:

$$J_{mem,acl} = \frac{2.5}{22}\frac{i_{fc}}{F}\lambda_2 - \frac{2\rho_{mem}}{M_{eq}}D(\lambda_2)\frac{\lambda_3-\lambda_2}{H_{mem}} \tag{1}$$

$$J_{mem,ccl} = \frac{2.5}{22}\frac{i_{fc}}{F}\lambda_4 - \frac{2\rho_{mem}}{M_{eq}}D(\lambda_4)\frac{\lambda_4-\lambda_3}{H_{mem}} \tag{2}$$

These three water contents are described by the three ODEs equations as:

$$\frac{d\lambda_2}{dt} = \frac{M_{eq}}{H_{cl}\rho_{mem}}\left(J_a - J_{mem,acl}\right) \tag{3}$$

$$\frac{d\lambda_3}{dt} = \frac{M_{eq}}{H_{mem}\rho_{mem}}\left(J_{mem,acl} - J_{mem,ccl}\right) \tag{4}$$

$$\frac{d\lambda_4}{dt} = \frac{M_{eq}}{H_{cl}\rho_{mem}}\left(J_{mem,ccl} + \frac{i_{fc}}{2F} - J_c\right) \tag{5}$$

The rate of desorption of water from the electrolyte is represented by the weighted average of the desorption rates of water vapor and liquid water:

$$\gamma = (1-w_l)\gamma_v + w_l\gamma_l \tag{6}$$

$$w_l = \frac{\lambda-14}{16.8-14}\cdot 0.5 + \frac{a_w-1}{3-1}\cdot 0.5, w_l \in [0,1] \tag{7}$$

where a_w is water activity in CL pores.

The electrolyte desorption water fluxes in ACL and CCL are expressed as:

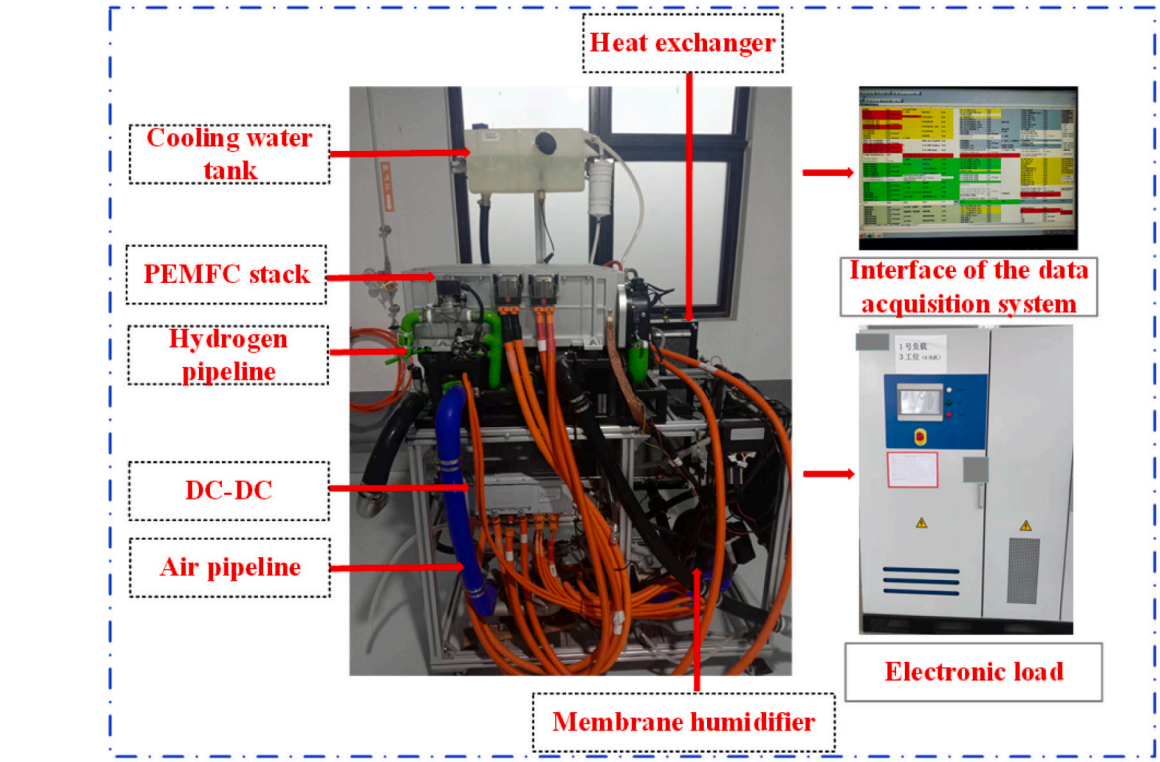

(a)

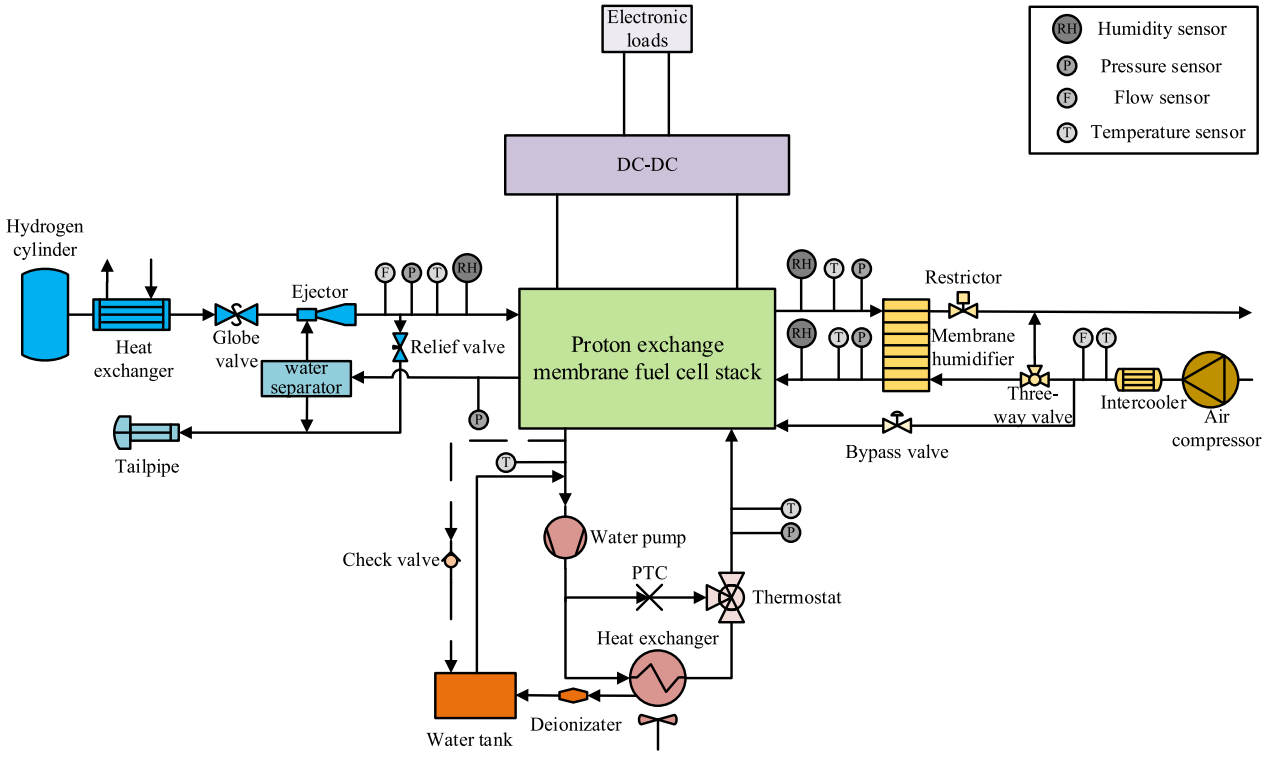

(b)

Fig. 1. PEMFC stack: (a) experimental platform; (b) system principle diagram.

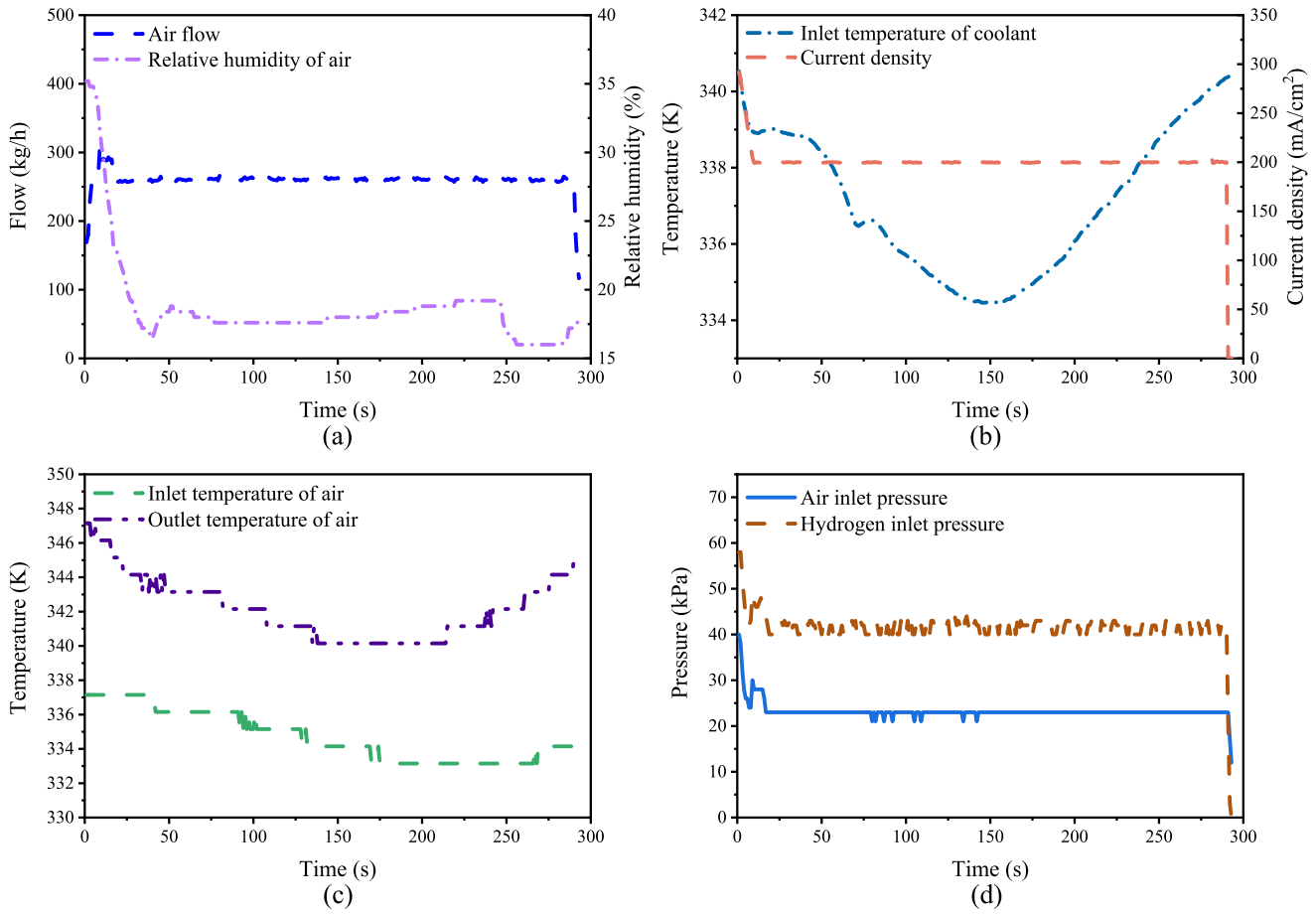

Fig. 2. Main operating parameters during shutdown purge: (a) air flow rate and RH; (b) cooling water inlet temperature and current density; (c) purge air inlet/outlet temperature; and (d) air/hydrogen inlet pressure.

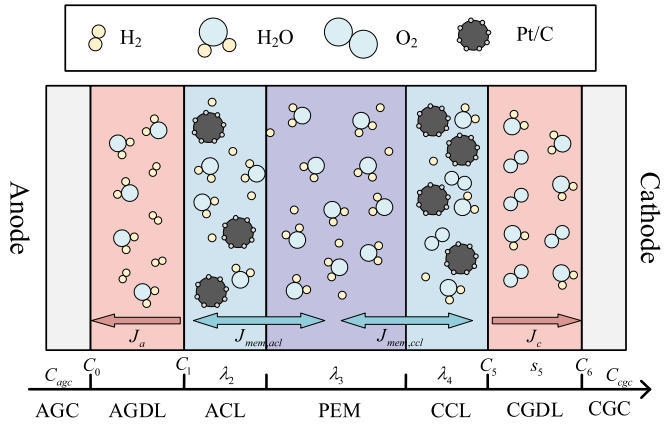

Fig. 3. Simulation model computational domain.

$$J_a = \gamma_v \varepsilon_{cl} H_{cl} \frac{\rho_{mem}}{M_{eq}} \left(\lambda_{eq,acl} - \lambda_2\right) \tag{8}$$

$$J_c = \gamma \varepsilon_{cl} H_{cl} \frac{\rho_{mem}}{M_{eq}} \left(\lambda_4 - \lambda_{eq,ccl}\right) \tag{9}$$

The molar concentration of water vapor within a porous medium can be expressed as in the following equation:

$$-D_{va} {\varepsilon_{gdl}}^{1.5} \cdot \frac{C_1 - C_0}{H_{gdl}} = hm_v \left(C_{agc} - C_0\right) = J_a \tag{10}$$

Table 1
Key parameters.

Description	Value	Unit
CL porosity	0.6	
GDL porosity	0.6	
Equivalent weight of membrane	1.1	kg/mol
Water molecular weight	0.018	kg/mol
Vapor diffusivity in cathode	2.236×10^{-5}	m^2/s
Vapor diffusivity in anode	5.457×10^{-5}	m^2/s
Convective mass transfer coefficient	0.08	m/s
GDL permeability	6.875×10^{-13}	m^2
Gas dynamic viscosity	1×10^{-5}	Pa s
Contact angle of GDL	110	◦
Dry density of membrane	1980	kg/m^3
Water density	1000	kg/m^3
Surface tension	0.0625	N/m
Universal gas constant	8.314	J/(mol•K)
Faraday constant	96,487	C/mol
GDL thickness	2×10^{-4}	m
CL thickness	1×10^{-5}	m
Membrane thickness	2.5×10^{-5}	m
Channel height	1×10^{-3}	m
Channel length	0.62	m
Active area	0.025	m^2

$$D_{vc} {\varepsilon_{gdl}}^{1.5} \cdot \frac{C_5 - C_6}{H_{gdl}} = hm_v \left(C_6 - C_{cgc}\right) = J_c - J_{cl} \tag{11}$$

Liquid water saturation is an important parameter in describing the liquid transport, where the volume of liquid occupied in the pores can be expressed by the following equation [28]:

$$\rho_l \frac{dV_l}{dt} = -q_l - kM_{H_2O}\varepsilon V_{gdl} \tag{12}$$

where q_l is mass flow rate of liquid water, k is evaporation condensation factor, V_{gdl} is total volume of the gas diffusion layer.

The mass flow rate of liquid water can be expressed by the following equation as [29]:

$$q_l = \frac{AKK_{rl}}{\eta_l}\left|\frac{dP_c}{ds_r}\right|\frac{s_r}{H_{gdl}} \tag{13}$$

The classical voltage model can be expressed as the difference between the open-circuit voltage and the three types of losses [30], which can be expressed as in the following equation:

$$U_{fc} = U_0 - (v_{act} + v_{ohmic} + v_{conc}) \tag{14}$$

where U_{fc} is actual voltage at current operating conditions.

Regarding the activation polarization loss can be derived from the Butler-Volmer equation:

$$v_{act} = \frac{RT}{\alpha F} ln\left(\frac{i_{fc}}{i_0}\right) \tag{15}$$

The ohmic polarization can be expressed in the form of a product between the fuel cell current density and the electron conduction resistance and proton conduction resistance [31]:

$$v_{ohmic} = i_{fc}(r_e + r_p) \tag{16}$$

where r_p and r_e are the proton conduction resistance and the electron conduction resistance.

The concentration polarization can be expressed as in the following equation:

$$v_{conc} = \frac{RT}{nF}\left(1 + \frac{1}{\alpha}\right) ln\left(\frac{i_L}{i_L - i}\right) \tag{17}$$

where i_L is the limiting current density.

3. Results and discussion

3.1. Effect of purge conditions at high stack temperatures on the purge process

This section examines how high stack temperatures influence the PEMFC shutdown purge process. The analysis focuses on the variation of critical parameters such as cell voltage and HFR during the purge. Fig. 4 displays the variation of cell parameters during the PEMFC shutdown purge. As shown in Fig. 4 (a), the voltage of a single cell decreases steadily during the purge, dropping from its initial value to 0.66 V after approximately 150 s. This voltage decrease is attributed to the effective removal of water content within the cell, which increases proton conduction resistance. During the initial 150 s, the cooling water outlet temperature continuously decreases from 344.2 K to 334.4 K. This temperature drop slows the rate of voltage change as it partially counteracts the evaporation capacity. When the thermostat of the cell cooling water circuit shuts off at 150 s, the internal temperature of the cell rapidly rises to 343.8 K. This higher temperature accelerates the removal of water, causing the cell voltage to further decline to 0.34 V in post-purge.

Fig. 4(b) illustrates the variation of the HFR curve of the average single cell during the purge process. As purging proceeds, the HFR of the cell increases, indicating effective water removal from the cell. Similarly, the HFR increases more slowly during the first 150 s due to the continuous decrease in cooling water outlet temperature. When the thermostat closes, the internal cell temperature rises rapidly, causing a swift reduction in internal water content and a corresponding rapid increase in HFR. Due to the sustained high stack temperature during purging, the HFR of the single cell eventually reaches 639.44 mΩ•cm^2, far exceeding the safety threshold of 500 mΩ•cm^2 provided by the stack supplier. This high-temperature purge process causes severe and irreversible damage to the stack.

The high-temperature purge process causes significant damage to the fuel cell stack, as depicted in Fig. 5. Fig. 5 (a) depicts the over-drying inside some cells due to elevated temperatures during the purge process, leading to significant perforation of the MEAs in those cells. Furthermore, as shown in Fig. 5(b), the voltages of two single cells were 0.99 V and 0.97 V, respectively, upon restarting the stack, which is significantly lower than the normal single cell voltage. The damage to the fuel cell interior caused by prolonged high-temperature purging is severe and irreversible.

3.2. Analysis of internal water content affected by different cell temperatures

To understand how varying cell temperatures influence the effectiveness of the shutdown purge in a PEMFC, the internal water content under different thermal conditions was analyzed in this section. This analysis aims to identify the optimal temperature range for purging that ensures efficient water removal while maintaining cell integrity. To establish a baseline for comparison, we used a simulation model to determine the initial conditions before the purge. The steady-state operating parameters, detailed in Table 2, reflect a fully hydrated cell

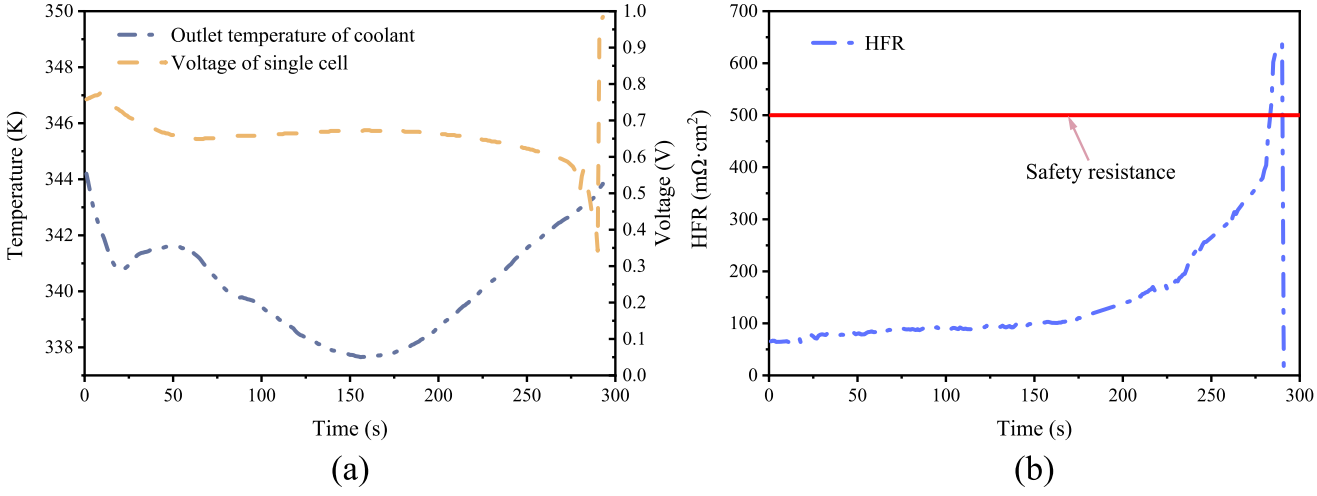

Fig. 4. Variation of parameters during shutdown purge: (a) single cell voltage and cooling water outlet temperature; (b) HFR curves of the single cell.

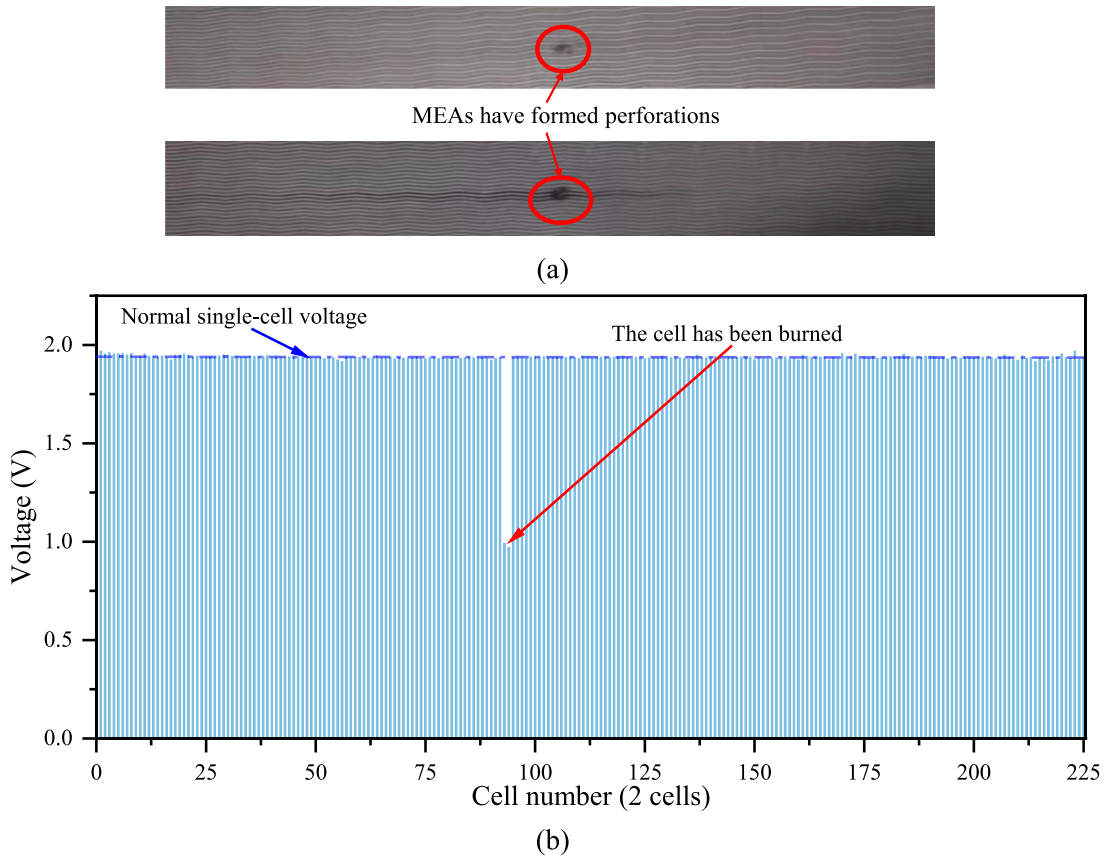

Fig. 5. Damage to the stack caused by high-temperature purge: (a) perforation of MEAs; (b) single cell voltage abnormality.

Table 2
Main operating parameters during steady-state operation of the fuel cell.

Parameters	Value	Unit
Relative humidity at anode side	60	%
Relative humidity at cathode side	60	%
Hydrogen stoichiometry	1.5	
Air stoichiometry	2.3	
Anode side inlet pressure	2.3	bar
Cathode side inlet pressure	2.1	bar
Fuel cell operating current density	1100	mA/cm^2
Fuel cell operating temperature	348.15	K

with a notable concentration gradient from the cathode to the anode. Before the shutdown purge, the electrolyte in the cell is fully hydrated, displaying a concentration gradient from the cathode side to the anode side. The membrane water content in the CCL, PEM and ACL are 19.70, 17.78 and 15.83, respectively. In the cell, the water concentration decreases from the electrolyte towards both side channels. The porous medium on the cathode side is saturated with vapor and the liquid water saturation is 0.123.

The main purge parameters used in this study are shown in Table 3.

Table 3
Main operating parameters of the purge phase of a fuel cell.

Parameters	Value	Unit
RH at anode side	30	%
RH at cathode side	30	%
Hydrogen stoichiometry	1.5	
Air stoichiometry	10	
Anode inlet pressure	2.3	bar
Cathode inlet pressure	2.1	bar
current density	100	mA/cm^2

Various fuel cell temperatures were employed to investigate their effect on the purge process. To understand the effect of temperature more comprehensively, temperatures higher than those during the steady-state operation were used during the purge process. In total, 12 groups of cell temperatures were used: 303.15 K, 308.15 K, 313.15 K, 318.15 K, 323.15 K, 328.15 K, 333.15 K, 338.15 K,343.15 K, 348.15 K, 353.15 K, and 358.15 K. These varied temperatures provide insights into how temperature influences the purge process's efficiency and safety.

Considering factors such as power loss and user wait time, a purge time of 120 s was selected for this study. Additionally, due to the varying binding strengths of water to SO_3^- in the electrolyte, there is tightly bound non-freezable water with a saturation limit of 4.8 [5]. In this study, it is considered that if there is no residual liquid water in the cell after 120 s of purge and the membrane water content is less than or equal to 4.8, the shutdown purge effectively prevents icing problems.

3.2.1. Effect of cell temperature on membrane water content during purge process

In this section, how cell temperature affects membrane water content during PEMFC shutdown purge is explored. Understanding these effects is crucial for optimizing the purge process to avoid damage caused by damage due to over-drying or over-wetting.

Fig. 6 illustrates how the membrane water content changes over time at various cell temperatures during the purge. The data indicates that the ability to purge diminishes at lower temperatures. Notably, when the cell temperature drops below 308.15 K, the membrane water content post-purge is higher than before the purge, indicating inadequate water removal. At low temperatures, the desorption behavior and internal transport capacity of the membrane are weakened, resulting in the accumulation of water in the membrane. The purge curves show steeper slopes at higher temperatures, reflecting a more significant reduction in water content. This enhanced water removal efficiency at elevated

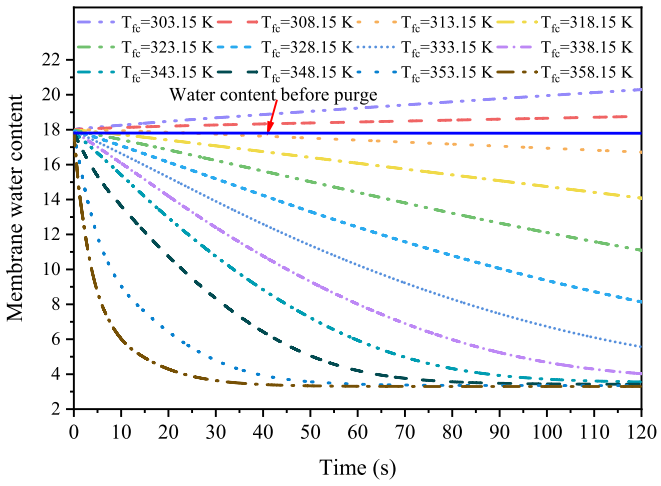

Fig. 6. Purge curves of membrane water at different cell temperatures.

temperatures is due to the increased rate of water diffusion within the membrane and higher water activity, which facilitates the transfer of water from the electrolyte into the porous medium. Consequently, higher cell temperatures enhance the membrane's dehydration capacity when other purge parameters are held constant.

The residual membrane water content after purge at different cell temperatures is shown in Fig. 7. When the cell temperature decreases from 358.15 K to 303.15 K, the residual water content in the membrane after 120 s of purge is 20.296, 18.764, 16.713, 14.082, 11.096, 8.139, 5.565, 4.027, 3.558, 3.423, 3.349, and 3.295, respectively. For temperatures between 338.15 K to 358.15 K, the residual membrane water after the purge is below 4.8, suggesting that this range can theoretically be used for fuel cell purging. However, comparing the slopes of the purge curves for different cell temperatures in Fig. 6 reveals that the difference in slope between 343.15 K and 338.15 K is minimal. Thus, temperatures above 338.15 K are less significant based on considerations tolerance of the purge process to temperature variations. Additionally, experimental analyses in Section 3.1 indicate that prolonged use of high-temperature purge can be very damaging to the cell. Therefore, considering various factors, a cell temperature of 338.15 K is the most effective for purging membrane water under the purge conditions in this paper.

The rate of change of membrane water content with cell temperature in Fig. 7 is based on the stable operating temperature of 348.15 K, where the "−" indicates an increase in membrane water content. Compared to a direct purge at 348.15 K, the membrane water content decreases by 2.13 % and 3.73 % after 120 s of purge when the cell temperature is elevated by 5 K and 10 K, respectively. Thus, raising the cell temperature above the normal operating temperature during purging offers little benefit. Conversely, lowering the cell temperature by 5 K, 10 K, 15 K, 20 K, 25 K, 30 K, 35 K, 40 K, and 45 K increases the membrane water content in post-purge by 3.94 %, 17.67 %, 62.59 %, 137.81 %, 224.20 %, 311.43 %, 388.30 %, 448.24 %, and 493.01 %, respectively. Therefore, the purge should be completed before the cell temperature drops much.

In addition, when the cell temperature was in the range of 338.15 K to 358.15 K, the changes in membrane water content after 120 s of purge were all within 5 %, and the residual membrane water content was basically the same. This is mainly due to the fact that the nature of the fuel cell shutdown purge is a dynamic equilibrium between internal water generation and discharge. In terms of the ability of water to drain out of the stack, this ability is mainly affected by factors such as the stoichiometric ratio, RH, and pressure, and in the absence of a change in these factors, the ability of water to drain out of the interior of the cell does not change. In terms of the ability of the fuel cell to generate water internally, while the temperature of the cell can certainly affect the rate of internal electrochemical reactions, the small current density of the purge process results in a small effect of the cell temperature on the ability to generate water. In summary, simply changing the cell temperature during purge does not significantly affect the ability to generate and discharge water.

3.2.2. Effect of cell temperature on the water content within porous media during purging

In this section, the effect of cell temperature on water content in porous media is investigated during purge. The analysis focuses on the conversion of membrane water into vapor and liquid phases and their subsequent behaviors under varying temperature conditions. In the fuel cell model examined, the electrochemical reaction primarily produces water in the electrolyte of the CCL. Consequently, the water produced is in the membrane, where it is subsequently converted to vapor and liquid water through desorption from the electrolyte into the porous medium. The rates of desorption for vapor and liquid within the membrane differ. This study employs weighted average coefficients (w_l) to simplify the quantification and rate of membrane water conversion to vapor and liquid, respectively.

The variation of w_l for membrane water conversion with time at

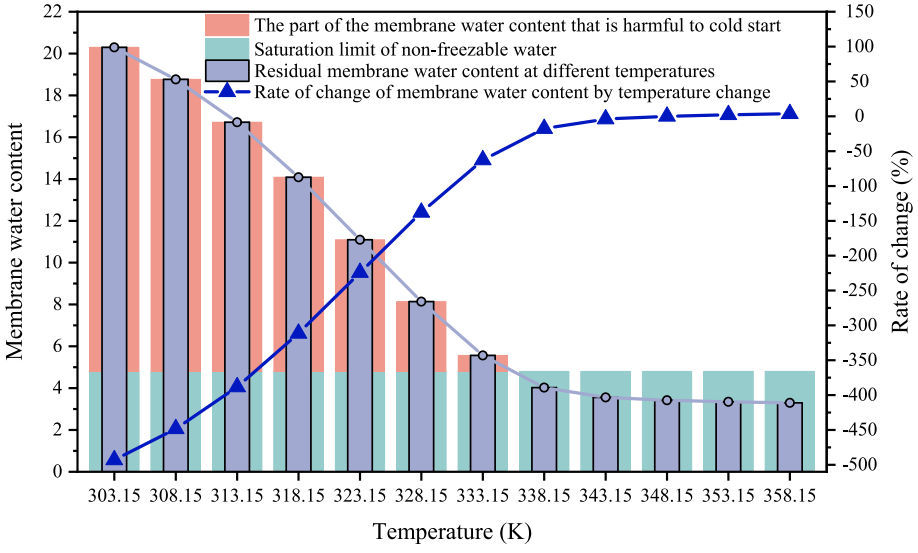

Fig. 7. Residual membrane water content after purge at different cell temperatures.

different cell temperatures is shown in Fig. 8. When w_l equals 1, the membrane mainly desorbs liquid water to the porous medium, while w_l equal to 0 indicates a predominant desorption of vapor. Fig. 8 demonstrates that cell temperature significantly influences the state of desorbed water from the membrane. The w_l is primarily determined by the membrane's water content and water activity. At the same water content, higher temperatures increase water activity, favoring the desorption of vapor.

Fig. 9 illustrates how liquid water content on the cathode side varies with time across different cell temperatures. Within the temperature range of 358.15 K to 323.15 K, no liquid water remained in the porous media after purging. The time required for complete removal of liquid water at these temperatures was 2.001 s, 4.009 s, 16.333 s, 22.337 s, 31.384 s, 45.988 s, and 72.453 s, respectively. This phenomenon is primarily due to the fact that the saturated vapor pressure of water increases with temperature under typical fuel cell conditions. At higher temperatures, liquid water rapidly evaporates into vapor.

However, when the cell temperature ranged from 328.15 K to 303.15 K, purging for 120 s did not completely remove the liquid water from the cell. The saturation of residual liquid water in the post-purge was 0.008, 0.0505, 0.104, and 0.187, respectively. At 303.15 K, the liquid water content within the porous medium is higher than during normal operation. This phenomenon occurs because lower cell temperatures result in lower saturation vapor pressures, weakening the ability of liquid water to evaporate, even vapor condenses into liquid. Additionally, as shown in Fig. 8, lower cell temperatures decrease water activity, making the membrane more inclined to desorb liquid water. This explains the decrease in the slope of the liquid water purge curve with decreasing temperature. In conclusion, as the cell temperature decreases, removing liquid water becomes more difficult.

Fig. 10 shows the variation in the phase transition coefficient of water during the purge process for different cell temperatures. The phase transition coefficient reflects the rate of water phase changes, with positive values indicating evaporation and negative values indicating condensation. Fig. 10 (a) shows the phase transition coefficient's variation with purge time for different cell temperatures, while Fig. 10 (b) shows the peak value of the phase transition coefficient at different cell temperatures. In the purge model of this study, since the purge parameters and cell temperature change abruptly, vapor condenses rapidly when the cell temperature is below 348.15 K. The peak condensation coefficients at cell temperatures from 303.15 K to 343.15 K are −10,483.68, −10,022.87, −9447.54, −8735.78, −7862.84, −6801.03, −5519.52, −3984.31, and − 2158.10, respectively. As the concentration of condensable vapor decreases, the condensation coefficient starts to decline. Due to the different saturated vapor pressures of water at various temperatures, higher cell temperatures lead to a faster decrease in the condensation coefficient.

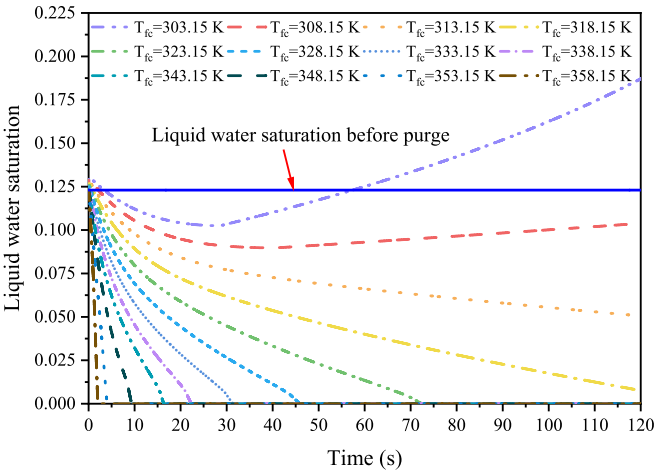

Fig. 9. Purging curves of liquid water on the cathode side at different cell temperatures.

As the purge proceeds, liquid water at all cell temperatures begins to evaporate once the phase change caused by the changing purge parameters stabilizes. After reaching a peak, the evaporation coefficient decreases until the evaporation of liquid water ends. The peak evaporation coefficient increases with cell temperature, with values at 303.15 K to 358.15 K being 129.68, 173.72, 229.19, 298.52, 384.69, 491.41, 623.33, 786.44, 988.37, 1262.01, 1947.24, and 4300.47, respectively. Additionally, the time to phase transition equilibrium decreases with increasing cell temperature because the total amount of water produced and removed does not significantly change. Due to the 120-s purge time limitation, liquid water can only be evaporated when the cell temperature is between 323.15 K and 358.15 K, consistent with Fig. 9.

The purge curves of vapor on the cathode side at different cell temperatures are shown in Fig. 11. The sudden change in temperature leads to a drastic change in vapor concentration at the start of the purge. Because of the different saturated vapor pressures of water at varying

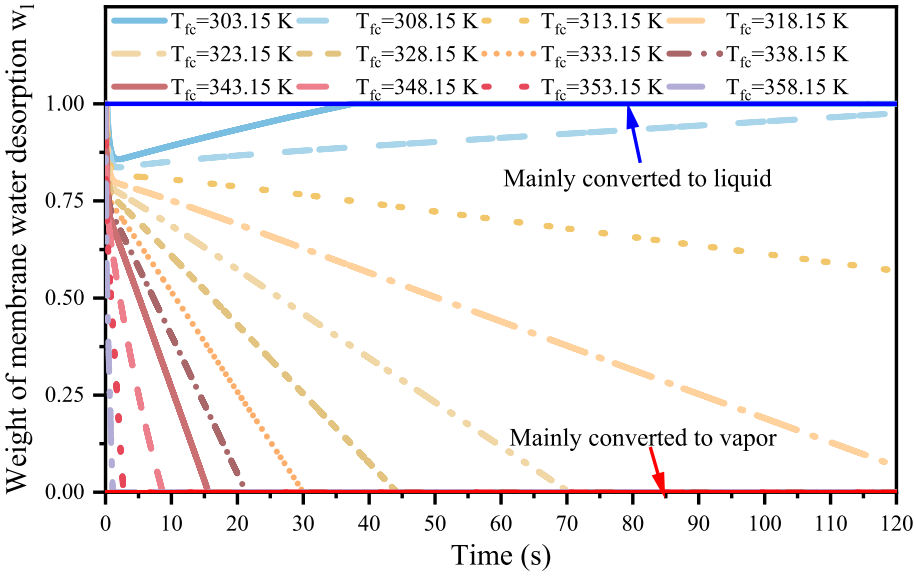

Fig. 8. Weights of membrane absorption as a function of time.

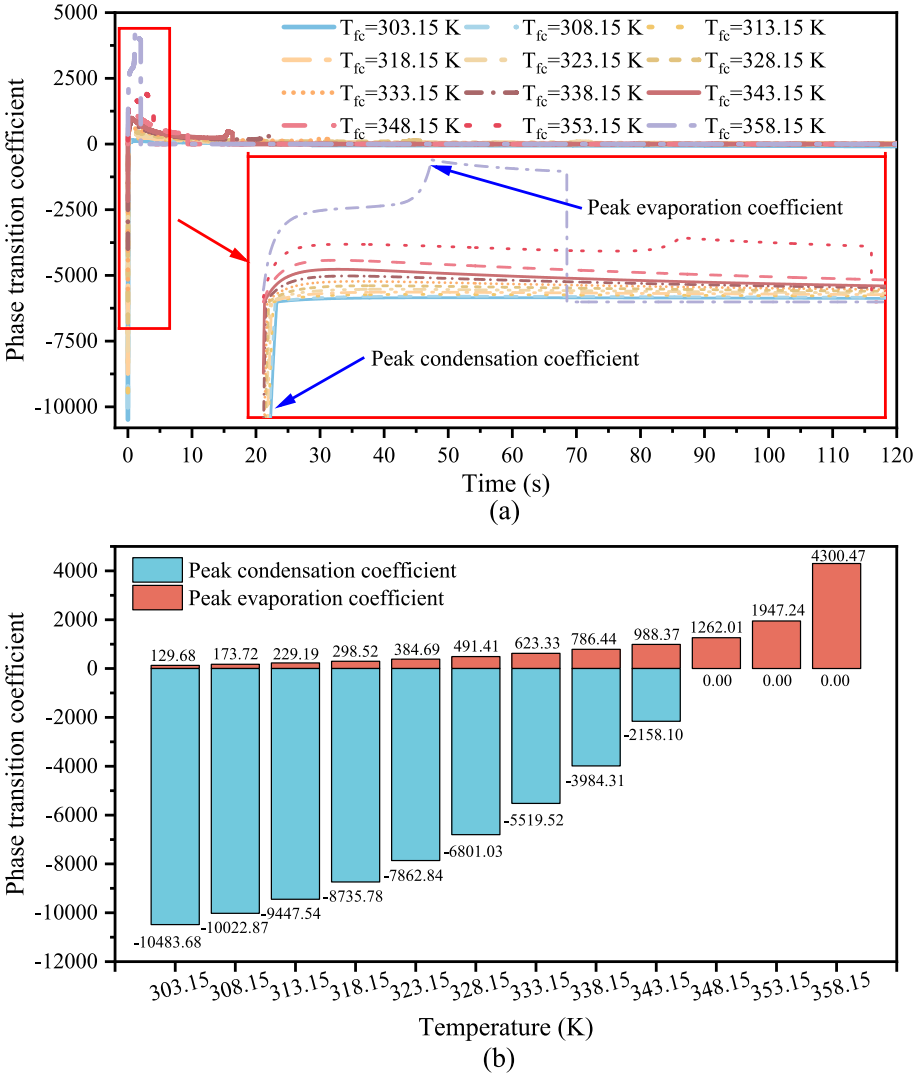

Fig. 10. Variation of phase transition coefficient of water during purge: (a) Variation of phase transition coefficient with purge time for different cell temperatures; (b) Peak values of phase transition coefficient for different cell temperatures.

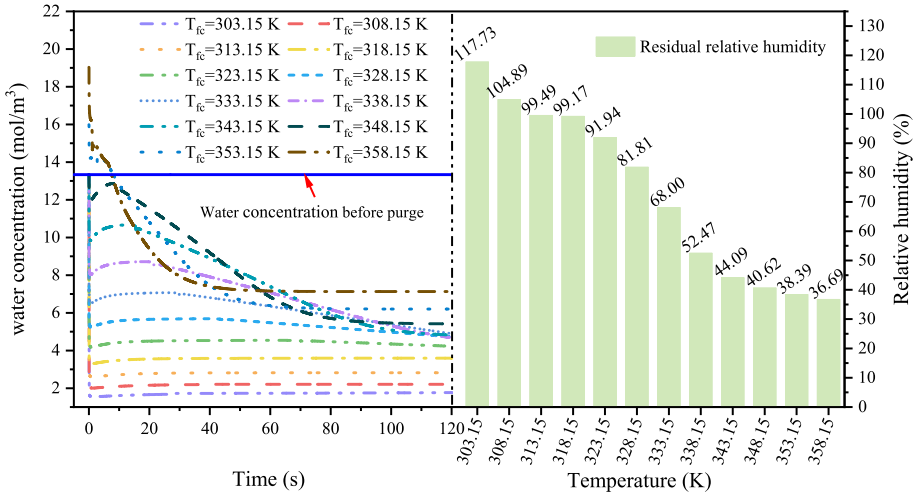

Fig. 11. Vapor purge curves and residual RH on the cathode side at different cell temperatures.

temperatures, a sudden temperature change in the cell causes a significant phase transition between water vapor and liquid water. The cathode side vapor concentration at temperatures from 303.15 K to 348.15 K decreases rapidly to: 1.541 mol/m^3, 2.003 mol/m^3, 2.581 mol/m^3, 3.295 mol/m^3, 4.169 mol/m^3, 5.231 mol/m^3, 6.508 mol/m^3, 8.032 mol/m^3, 9.837 mol/m^3, and 11.931 mol/m^3, respectively. At cell temperatures of 353.15 K and 358.15 K, the vapor concentration quickly increases to 15.989 mol/m^3 and 19.032 mol/m^3, respectively. Additionally, the residual vapor concentration in post-purge increases with temperature. However, since the saturation vapor pressure is positively correlated with the temperature, the RH inside the porous medium at the cathode side tends to decrease with increasing cell temperature, as shown in Fig. 11. The RHs at the cathode side are 117.73 %, 104.89 %, 99.49 %, 99.17 %, 91.94 %, 81.81 %, 68.00 %, 52.47 %, 44.09 %, 40.62 %, 38.39 %, and 36.69 %, respectively.

4. Conclusions and future studies

This study utilized an integrated experimental platform comprising 450 cells to investigate the impact of high-temperature purges on the performance and potential damage to PEMFCs. To analyze how varying cell temperatures affect the shutdown purge process, an isothermal, transient, two-phase flow PEMFC model was developed using MATLAB/SIMULINK to simulate the purge process lasting 120 s. The focus was on understanding the phase transitions of water during the purge, including membrane desorption and gas-liquid transitions. The key findings are summarized as follows:

(1) In terms of membrane water removal, both the diffusion and water activity within the membrane decrease as the cell temperature decreases, leading to a diminished capacity to purge water effectively. Consequently, the residual water content in the membrane after purging increases with decreasing temperature. At higher temperatures, water is predominantly desorbed as vapor, enhancing the purge process's effectiveness. In contrast, at lower temperatures, liquid water desorption is more common, making it harder to remove water from the membrane.
(2) The ability to purge liquid water declines as the cell temperature drops. Specifically, within the temperature range of 303.15 K to 318.15 K, the study found that liquid water could not be entirely purged within 120 s. Notably, at 303.15 K, the liquid water content post-purge exceeded that during normal operation due to the low saturated vapor pressure of the water, highlighting a significant challenge at lower temperatures.
(3) Due to the positive correlation between saturated vapor pressure and temperature, as the cell temperature rises, despite the residual vapor concentration after purge increases, the RH within the porous medium decreases, reflecting more efficient water evaporation and removal. Furthermore, the time to achieve phase transition equilibrium shortens with rising cell temperature.
(4) The study revealed that temperature primarily influences the phase transitions among gas, liquid, and membrane water by affecting saturated vapor pressure and water activity. While raising the cell temperature increases the purge rate, its effect on the absolute water content remaining in the cell post-purge is relatively minor. Furthermore, the rapid evaporation and removal of water from the cell by the continuous high-temperature purge is highly susceptible to irreversible damage such as MEA perforation.

Based on the insights gained from this study, to balance effective water removal, energy efficiency, and minimize damage to the cell, the study suggests maintaining a purge temperature of 338.15 K. This temperature optimizes the purge process while avoiding the detrimental effects associated with prolonged high-temperature exposure. Additionally, the increase in absolute concentration of residual vapor with increasing cell temperature found in this study may lead to the problem of internal water redistribution during natural cooling of the cell after purge, which may be an interesting topic to be explored in future studies. Finally, developing advanced materials or coatings that can endure high-temperature conditions could significantly extend the operational life and enhance the performance of PEMFCs.

CRediT authorship contribution statement

Zhenya Zhang: Writing – original draft, Software, Methodology, Investigation, Funding acquisition, Formal analysis, Data curation, Conceptualization. **Houyu Wei:** Writing – original draft, Software, Methodology, Investigation. **Taishan Lou:** Writing – original draft, Methodology, Investigation. **Jun Zhang:** Writing – original draft, Methodology, Investigation. **Yanqiu Xiao:** Writing – original draft, Methodology, Investigation. **Tingxiang Jin:** Writing – original draft, Methodology, Investigation. **Jiean Tian:** Writing – original draft, Methodology, Investigation. **Xuewei Li:** Writing – original draft, Methodology, Investigation. **Zhengxuan Liu:** Writing – review & editing, Writing – original draft, Supervision, Software, Methodology, Investigation, Formal analysis, Data curation, Conceptualization.

Declaration of competing interest

The authors declare that they have no known competing financial interests or personal relationships that could have appeared to influence the work reported in this paper.

Data availability

Data will be made available on request.

Acknowledgements

This work was supported by the Key Scientific Research Projects in Colleges and Universities in Henan Province (Grant No.24A470013), and the Key Research and Development Program of Henan Province (Grant No. 241111222900).

References

[1] F. Cai, S. Cai, Z. Tu, Proton exchange membrane fuel cell (PEMFC) operation in high current density (HCD): problem, progress and perspective, Energ. Convers. Manage. 307 (2024) 118348, https://doi.org/10.1016/j.enconman.2024.118348.
[2] R.J. Yu, H. Guo, H. Chen, F. Ye, Heat and mass transfer at the interface between cathode catalyst layer and gas diffusion layer of a proton exchange membrane fuel cell, Int. Commun. Heat Mass Transf. 140 (2023) 106548, https://doi.org/10.1016/j.icheatmasstransfer.2022.106548.
[3] Z. Zhang, J. Mao, Z. Liu, Advancements and insights in thermal and water management of proton exchange membrane fuel cells: challenges and prospects, Int. Commun. Heat Mass Transf. 153 (2024) 107376, https://doi.org/10.1016/j.icheatmasstransfer.2024.107376.
[4] Z.R. Guo, H. Chen, H. Guo, F. Ye, Dynamic response and stability performance of a proton exchange membrane fuel cell with orientational flow channels: an experimental investigation, Energ. Convers. Manage. 274 (2022) 116467, https://doi.org/10.1016/j.enconman.2022.116467.
[5] Y. Luo, K. Jiao, Cold start of proton exchange membrane fuel cell, Prog. Energy Combust. Sci. 64 (2018) 29–61, https://doi.org/10.1016/j.pecs.2017.10.003.
[6] Y. Chen, L. Chen, W.-Q. Tao, Impact of Schroeder's paradox on cold start-up failure of proton exchange membrane fuel cells: three-dimension simulation based on OpenFOAM, Int. Commun. Heat Mass Transf. 146 (2023) 106914, https://doi.org/10.1016/j.icheatmasstransfer.2023.106914.
[7] S. Xu, F. Dong, C. Yang, B. Yin, A novel multi-physics pore-scale model of multiphase reactive flow and heat transfer at subzero temperatures in the gas diffusion layer of proton exchange membrane fuel cells, Int. Commun. Heat Mass Transf. 156 (2024) 107672, https://doi.org/10.1016/j.icheatmasstransfer.2024.107672.
[8] Z. Liu, H. Chen, T. Zhang, Review on system mitigation strategies for start-stop degradation of automotive proton exchange membrane fuel cell, Appl. Energy 327 (2022) 120058, https://doi.org/10.1016/j.apenergy.2022.120058.
[9] E. Cho, J.-J. Ko, H.Y. Ha, S.-A. Hong, K.-Y. Lee, T.-W. Lim, I.-H. Oh, Effects of water removal on the performance degradation of PEMFCs repetitively brought to <0°C, J. Electrochem. Soc. 151 (2004), https://doi.org/10.1149/1.1683580.

[10] S. Xu, B. Yin, Z. Li, F. Dong, A review on gas purge of proton exchange membrane fuel cells: mechanisms, experimental approaches, numerical approaches, and optimization, Renew. Sust. Energ. Rev. 172 (2023) 113071, https://doi.org/10.1016/j.rser.2022.113071.
[11] S.I. Kim, N.W. Lee, Y.S. Kim, M.S. Kim, Effective purge method with addition of hydrogen on the cathode side for cold start in PEM fuel cell, Int. J. Hydrogen Energ. 38 (2013) 11357–11369, https://doi.org/10.1016/j.ijhydene.2013.06.101.
[12] Y. Oh, S.-K. Kim, S. Lim, D.-H. Jung, D.-H. Peck, Y. Shul, The effects of freeze-thaw cycling and gas purging on performance degradation in direct methanol fuel cells, Int. J. Hydrogen Energ. 37 (2012) 17268–17274, https://doi.org/10.1016/j.ijhydene.2012.08.081.
[13] S.-Y. Lee, S.-U. Kim, H.-J. Kim, J.H. Jang, I.-H. Oh, E.A. Cho, S.-A. Hong, J. Ko, T.-W. Lim, K.-Y. Lee, T.-H. Lim, Water removal characteristics of proton exchange membrane fuel cells using a dry gas purging method, J. Power Sources 180 (2008) 784–790, https://doi.org/10.1016/j.jpowsour.2008.01.009.
[14] L. Shi, X. Tang, S. Xu, M. Zheng, Comprehensive analysis of shutdown purge influencing factors of proton exchange membrane fuel cell based on water heat transfer and water vapor phase change mechanism, Appl. Therm. Eng. 239 (2024) 122175, https://doi.org/10.1016/j.applthermaleng.2023.122175.
[15] H. Pan, L. Xu, S. Cheng, W. Sun, J. Li, M. Ouyang, Control-oriented modeling of gas purging process on the cathode of polymer electrolyte membrane fuel cell during shutting down, Int. J. Hydrogen Energ. 42 (2017) 18584–18594, https://doi.org/10.1016/j.ijhydene.2017.04.191.
[16] L. Shi, P. Liu, M. Zheng, S. Xu, Numerical study on the mechanism of water and gas phase transition and water redistribution after purging based on two-dimensional multi-phase model, Energ, Convers. Manage. 278 (2023) 116725, https://doi.org/10.1016/j.enconman.2023.116725.
[17] F. Wang, H. Zhang, M. Liu, X. Zhang, D. Yang, C. Zhang, An effective PEMFC system shutdown purge strategy for improving the purging effect of liquid water and the dehydration of stack, Int. J. Hydrogen Energ. 48 (2023) 28891–28905, https://doi.org/10.1016/j.ijhydene.2023.04.060.
[18] Y. Pei, F. Chen, J. Jiao, S. Liu, Analysis and control strategy design for PEMFC purging process, Energy 290 (2024) 130233, https://doi.org/10.1016/j.energy.2024.130233.
[19] Y.-T. Mu, P. He, J. Ding, W.-Q. Tao, Modeling of the operation conditions on the gas purging performance of polymer electrolyte membrane fuel cells, Int. J. Hydrogen Energ. 42 (2017) 11788–11802, https://doi.org/10.1016/j.ijhydene.2017.02.108.
[20] Y.S. Kim, S.I. Kim, N.W. Lee, M.S. Kim, Study on a purge method using pressure reduction for effective water removal in polymer electrolyte membrane fuel cells, Int. J. Hydrogen Energ. 40 (2015) 9473–9484, https://doi.org/10.1016/j.ijhydene.2015.05.136.
[21] W. Dai, H. Wang, X.-Z. Yuan, J.J. Martin, D. Yang, J. Qiao, J. Ma, A review on water balance in the membrane electrode assembly of proton exchange membrane fuel cells, Int. J. Hydrogen Energ. 34 (2009) 9461–9478, https://doi.org/10.1016/j.ijhydene.2009.09.017.
[22] K.T. Cho, M.M. Mench, Fundamental characterization of evaporative water removal from fuel cell diffusion media, J. Power Sources 195 (2010) 3858–3869, https://doi.org/10.1016/j.jpowsour.2009.12.084.
[23] K.T. Cho, M.M. Mench, Effect of material properties on evaporative water removal from polymer electrolyte fuel cell diffusion media, J. Power Sources 195 (2010) 6748–6757, https://doi.org/10.1016/j.jpowsour.2010.03.094.
[24] K. Tajiri, C.-Y. Wang, Y. Tabuchi, Water removal from a PEFC during gas purge, Electrochim. Acta 53 (2008) 6337–6343, https://doi.org/10.1016/j.electacta.2008.04.035.
[25] Z. Zhang, H. Wei, Y. Xiao, C. Cheng, J. Tian, X. Li, J. Liu, Z. Liu, Research on shutdown purge characteristics of proton exchange membrane fuel cells: purge parameters conspicuity and residual water, Appl. Therm. Eng. 249 (2024) 123437, https://doi.org/10.1016/j.applthermaleng.2024.123437.
[26] J. Hu, J. Li, L. Xu, F. Huang, M. Ouyang, Analytical calculation and evaluation of water transport through a proton exchange membrane fuel cell based on a one-dimensional model, Energy 111 (2016) 869–883, https://doi.org/10.1016/j.energy.2016.06.020.
[27] L. Xu, Z. Hu, C. Fang, L. Xu, J. Li, M. Ouyang, A reduced-dimension dynamic model of a proton-exchange membrane fuel cell, Int. J. Energy Res. 45 (2021) 18002–18017, https://doi.org/10.1002/er.6945.
[28] A.J. del Real, A. Arce, C. Bordons, Development and experimental validation of a PEM fuel cell dynamic model, J. Power Sources 173 (2007) 310–324, https://doi.org/10.1016/j.jpowsour.2007.04.066.
[29] J.H. Nam, M. Kaviany, Effective diffusivity and water-saturation distribution in single- and two-layer PEMFC diffusion medium, Int. J. Heat Mass Transf. 46 (2003) 4595–4611, https://doi.org/10.1016/s0017-9310(03)00305-3.
[30] M.W. Fowler, R.F. Mann, J.C. Amphlett, B.A. Peppley, P.R. Roberge, Incorporation of voltage degradation into a generalised steady state electrochemical model for a PEM fuel cell, J. Power Sources 106 (2002) 274–283, https://doi.org/10.1016/s0378-7753(01)01029-1.
[31] R. Makharia, M.F. Mathias, D.R. Baker, Measurement of catalyst layer electrolyte resistance in PEFCs using electrochemical impedance spectroscopy, J. Electrochem. Soc. 152 (2005), https://doi.org/10.1149/1.1888367.